Landslides
DOI 10.1007/s10346-024-02329-2

Kévin Elkharrat · Catherine Homberg · Sara Lafuerza · Nicolas Loget · Muriel Gasc-Barbier · Stephanie Gautier

Study cases of complex paleo-landslides in the south of France

Introduction

Complex paleo-landslides (Clague 2015; Francioni et al. 2017) or fossil landslides (Shultz and Harper 2002; Mather et al. 2003; Azañón et al. 2005) are considered as some quiescent geomorphic items in the current climatic and morphological conditions but capable of being reactivated with climate change that serves as a main catalyst (Zaruba and Mencl 1982). Only a few studies provide descriptions of complex paleo-landslides due to the challenge of identifying them. However, it has been shown that fossil landslides can serve as markers of extreme events to enhance our comprehension of the connection between landslide occurrences and weather patterns. Since the description of landslide mechanisms by Varnes (1978) and later works of Dikau et al. (1996) and Hungr et al. (2014), there are still some landslides that are challenging to classify. In particular, in multilayer environments, complex failures due to mechanical contrasts tend to develop (Zerathe and Lebourg 2012; Gutierrez et al. 2012; Pasuto and Soldati 2013). Thus, the typology of these paleo-landslides becomes crucial as it directly influences the definition of its failure model.

In the case of rock slopes, the stability is often controlled by the movement of joint-bounded blocks (Stead et al. 2006). Structural features such as faults and fractures can initiate landslides (Margielewski 2006). These types of landslides exhibit a complex failure mode including toppling and spreading movements, among others. Pre-existing vertical joint sets control the carbonate Larzac plateau (south of France), predisposing rock falls, rock topples, and rotational landslides of varying scales (Taboada et al. 2017). Joint monitoring reveals that deformation cycles of wedging and ratcheting due to thermomechanical creep induce permanent deformations responsible for the incremental downslope movements of rock columns (Taboada et al. 2017). These mechanical discontinuities are undoubtedly responsible for the hydraulic connectivity between the carbonates of the Larzac plateau and the underlying Triassic clays, as demonstrated by borehole monitoring in the Pegairolles-de-l'Escalette landslide (Denchik et al. 2019).

The present study aims to investigate two paleo-landslides affecting the Larzac plateau in the south of France on the Laurounet and Le Ricardenc river valleys, namely the Mont Mayres and the Lamerallède landslides (Fig. 1), respectively. In this study, we discuss their geometry and typology identified from field investigations and remote sensing surveys and compare them with structural geology. The potential triggering mechanism is proposed based on ^{36}Cl cosmogenic ages obtained on the preserved paleo-scarps or the upper edge of the slide mass.

Geological setting and methods

The Lamerallède and Mont Mayres landslides evolve in sedimentary rocks ranging from the highly fractured Jurassic (Hettangian) carbonate plateau to the Triassic (Ladinian) median sandstone via Triassic (Norian) evaporite clays (Fig. 1a). The Upper Hettangian dolomites, with a thickness of 200 m, consist of massive and tabular beds (ranging from one to several metres thick). In contrast, the Lower Hettangian rocks, positioned at the boundary with the Rhaetian, comprise a 15-m unit of superposed thin (5–10 cm thick) grey mudstone beds known as the "Parlatges" facies. Beneath it, the Rhaetian interval, a massive unit measuring 30–40 m in thickness, features thick dolomitized grainstones interspersed with marly intervals. The investigated landslides affect all the geological formations above the Norian-Carnian clays. The thickness of the Norian-Carnian clays is about 110 m, reaching locally 170 m. Additionally, the carbonate plateau experienced the influence of several low-throw faults with a north–south orientation (Fig. 1a). This carbonate plateau is also known to be karstified (Ambert and Ambert 1995).

Landslide mapping

Mapping of the landslides was based on field and remote sensing surveys. The French geographical survey (IGN, Institut Géographique National) gives LAS data files produced by LiDAR, which permit the production of a Digital Terrain Model (DTM). Thanks to IGN DTM, we produced hillshade maps used to map tectonic lineaments, also presented as rose diagrams (Fig. 2a and b). These data aim to investigate the potential link between instabilities and structural geology. To complete the landslides mapping, we performed field investigations on the Lamerallède and Mont Mayres landslides, which consisted of geological cartography, including bedding plane measurements (strikes and dips) on slide blocks. Field investigations also include a fracturing survey.

Exposure ages

We used the cosmogenic nuclide method with ^{36}Cl (Stone et al. 1996) for 13 samples to date scarps and the upper edge of the slide masses (Table 1). The Lamerallède landslide was sampled twice on its single scarp (Fig. 2a) (sites LAM1 and LAM2, respectively). The Mont Mayres landslide was sampled twice on the upper edge of the slide mass (sites MM1 and MM2, Fig. 2b). Site LAM1 was the only one sampled in the Lower Hettangian Parlatges Limestone, the others all being in the Upper Hettangian Dolomites. To quantify and correct for any topography shielding (Dunne et al. 1999), each dated surface's strike and dip and the horizon's elevation were measured every 20°. Exposure ages were computed following the methodology outlined by Schimmelpfennig et al. (2009), and scaling factors derived from Stone's model (Stone 2000) were employed. The

Published online: 14 August 2024

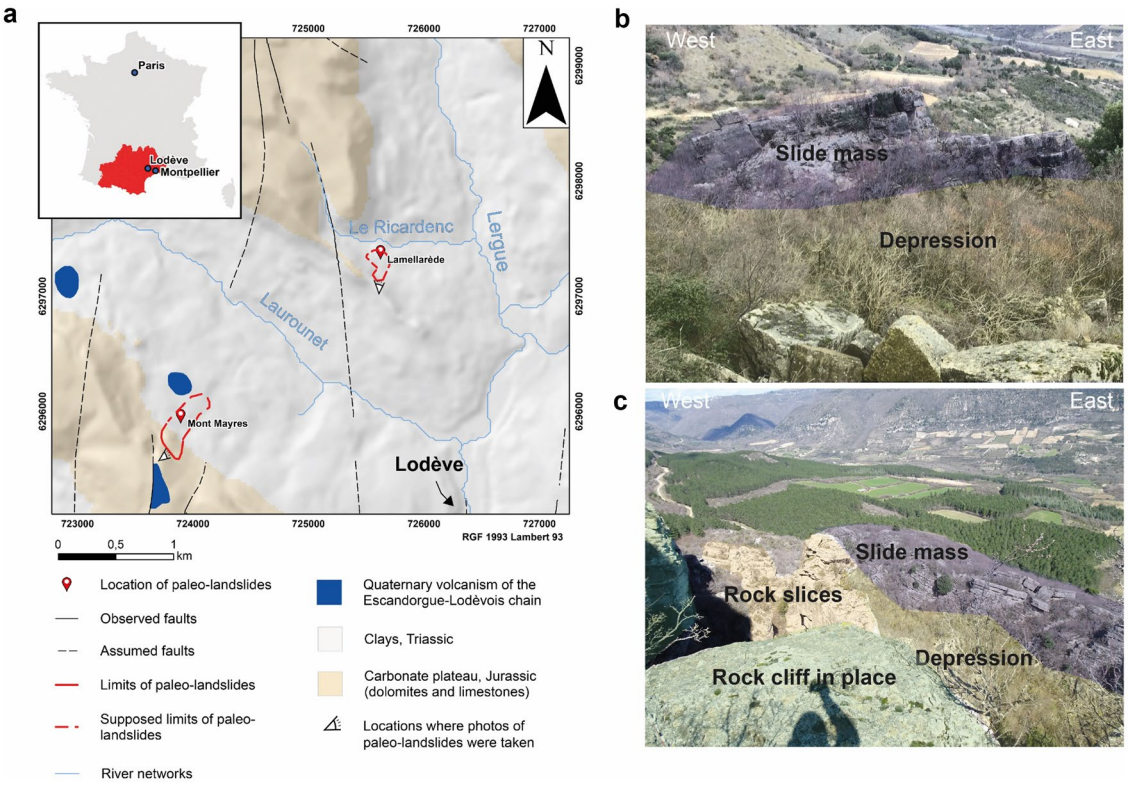

Fig. 1 **a** Simplified geological and structural map of the south of the Larzac plateau (the inset map shows France with the Occitanie region in red). Red bullets show the location of the investigated paleo-landslides on the map. **b** Photo of Lamerallède landslide. **c** Photo of Mont Mayres landslide

denudation rate was established at 0 mm. k. a^{-1}, assuming the surfaces to be non-eroded (Dunai 2010). All the dating data are documented in Table 1 and have been formatted following the guidelines provided by Dunai and Stuart (2009).

Results

Lamerallède landslide

Figure 2a shows the hillshade of the Lamerallède landslide (Fig. 1b) produced with the IGN LiDAR-derived DTM and geological data obtained in the field (bedding plane measurements and geological limits). From 380 to 410 m in altitude, a prominent slide mass is observed ahead of the rock cliff formed by the stiff Hettangian units (in-place geological units). The slide mass exposes in its upper part the succession of the Partlatges limestones (Early Hettangian) overlain by the massive dolomites (Late Hettangian) units. The Hettangian beds in the slide mass dip downslope by 20 to 30°, whereas the geological units in place are almost horizontal, with dips between 05°S and 09°W; despite the numerous joints that cut the carbonate units, the slide mass was not dismantled. The upward limit of the Lamerallède landslide is outlined by a 20-m-wide depression (indicated in yellow in Fig. 2a), filled by collapsed blocks of various sizes. Using the Lower/Upper Hettangian limit observed in the cliff (in place geological units) and in the landslide as a benchmark, the vertical offset is estimated to be 15 m. The scarp trace follows the depression, which trends at 070° and turns eastward to adopt a 130–140° strike. The bed strike of the slide mass may vary, but those with the more significant dips trend 060° in agreement with the N070 direction of the depression.

Below 380 m, the outcrop conditions are poor due to the vegetal cover. A dismantled mass is interpreted from the presence of isolated blocks. Moreover, cemented breccias at 350 m are observed. From a flat area to a high slope, the downslope morphology (Fig. 2a) outlines a topographic anomaly aligned with the upper part of the slide that we interpreted as a bulge defining the landslide toe.

Fracture measurement in in situ formations (Le Ricardenc Valley, Fig. 2) indicates two strike peaks. The first peak corresponds to a strike of 150–170°, and the second peak corresponds to a strike of 60–80°. These two sets of fractures are tectonic fractures because calcite has been found on their surface. The strike of the tilted beds in the slide mass coincides with the 60–80° fracture set, indicating that the E-W fractures played a role in the landslide initiation. The other set of fractures doesn't match the mobilization of the slide mass, but we can suppose that the N-S set cuts the slide mass. Fractures with 110°–130°N have also been recognized on the hillshade upward along the rock cliff. They are interpreted as a fracture zone that borders the rock cliff and may have guided the (lateral) western propagation of the landslide. Based on these geomorphological features, a geological cross-section has been proposed (Fig. 2c).

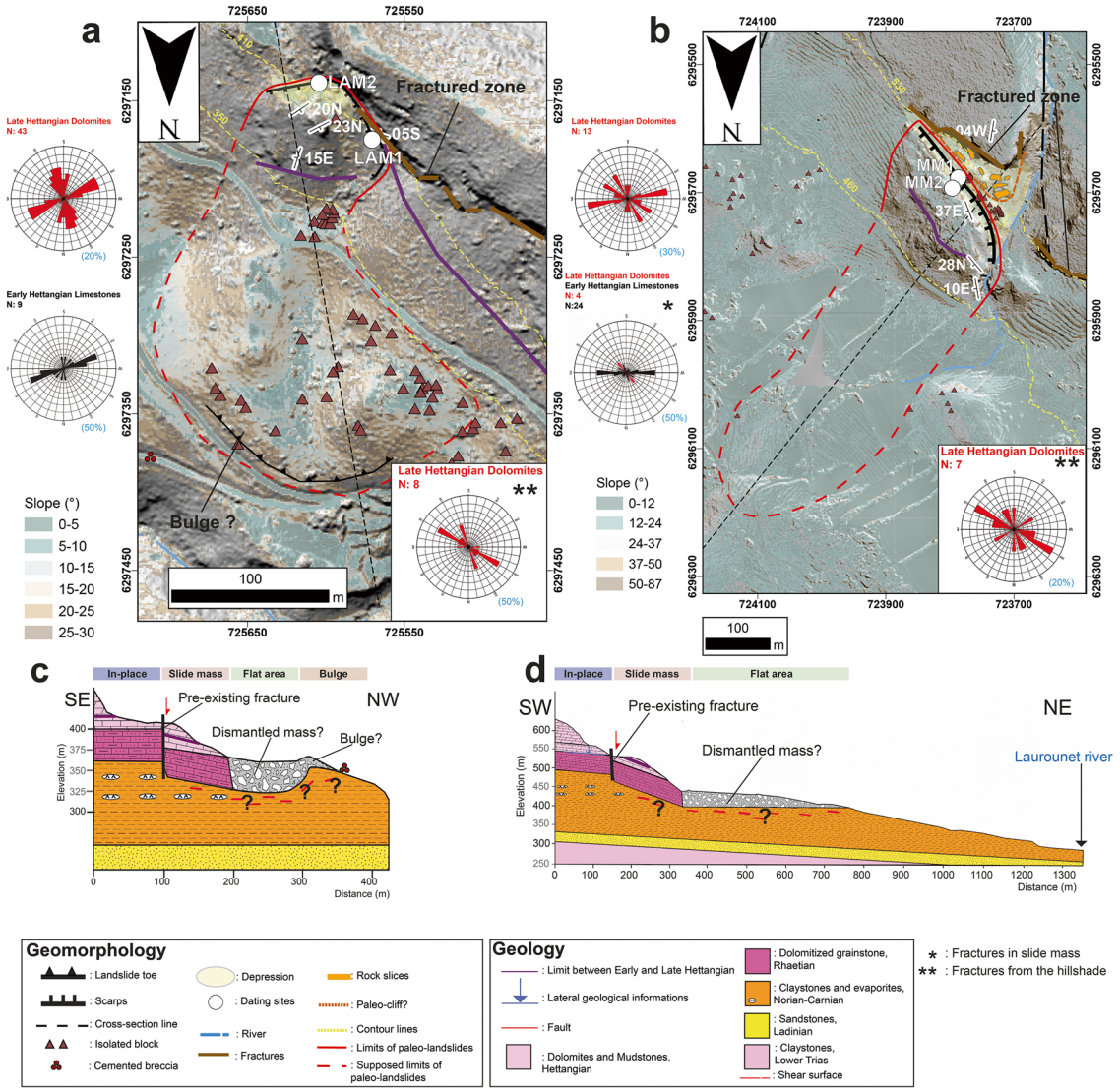

Fig. 2 Geology and geomorphology of Lamerallède and Mont Mayres landslides. **a** Hillshade produced by the Digital Terrain Model (DTM) of Lamerallède landslide with geomorphological features, bedding planes measurements, dating sites and geological limit between Lower and Upper Hettangian units. Inside a rose diagram (with % value of total of perimeter indicated in blue) is present with fractures located on the fractured zone on the DTM. Rose diagrams (with % value of total of perimeter indicated in blue) illustrate fracturing surveys performed during field investigations. **b** Hillshade was produced by the DTM of Mont Mayres landslide with geomorphological features, bedding plane measurements, dating site, and geological limit between Lower and Upper Hettangian units. Inside a rose diagram (with % value of total of perimeter indicated in blue) is present with fractures located on the fractured zone on the DTM. Rose diagrams (with % value of total of perimeter indicated in blue) illustrate fracturing surveys performed during field investigations. **c** Geological cross-section of Lamerallède landslide. **d** Geological cross-section of Mont Mayres landslide

Mont Mayres landslide

Figure 2b shows the hillshade of the Mont Mayres landslide (Fig. 1c). The Mont Mayres landslide outcrops well from 460-m to 530-m high (Fig. 2a). Below 530 m, the outcrops conditions are poor due to the vegetal cover. The slide mass identified is composed of Hettangian rocks ahead of the rock cliff and delimited by a major depression, which trends to 130–140°. As in the Lamerallède landslide, the Hettangian units in the slide mass dip downslope with an inclination generally more than 25° and up to 37°E. The strike of the bedding planes associated with these dips varies from 140 to 159°. Considering the 04–10° dip measured in the neighbouring in-place units (Fig. 2b), it is inferred that a significant bed tilt accompanied the movement of the Mont Mayres landslide. Preserving rock slices between the rock cliff and the landslide witness a damage zone now dismantled, not present in the Lamerallède landslide. Field observations allowed us to identify the limit between Lower and Upper Hettangian units in the slide mass only. Using lateral geological information, we estimated a 20 m offset (Fig. 2d). No bulge can be seen on the hillshade map or the field (Fig. 2b).

Table 1 ^{36}Cl AMS and ICP-MS measurements in the target fraction giving surfaces exposure ages calculated with topographic correction (S_T) with a denudation rate of 0 mm.kyr^{-1}

Site/Sample name		Lat (°)	Long (°)	Elev (m AMSL)	S_T	Cl (ppm)	Ca [wt%]	^{36}Cl/^{35}Cl (10^{-14}) with error (%)	N_{36} total (10^5 at.g^{-1})	^{36}Cl ages (kyr) o mm.kyr^{-1}
LAM1	LAM1a	43.773072	3.317658	415	0.5	128.82 ± 10.02	38.92 ± 0.98	2.25 ± 10.8	0.5 ± 0.06	2.79 ± 0.52
(Scarp)	LAM1b	43.773013	3.317503	415	0.51	186.68 ± 16.16	39.13 ± 1	2.97 ± 8.3	0.9 ± 0.1	4.57 ± 0.79
EHL	LAM1c	43.773102	3.317531	420	0.49	178.94 ± 21.59	38.98 ± 0.98	3.73 ± 8	1.01 ± 0.13	5.52 ± 1.05
	LAM1d	43.773111	3.317486	425	0.53	181.12 ± 21.57	38.91 ± 0.98	2.46 ± 9	0.68 ± 0.09	3.19 ± 0.64
									Mean	**4.01 ± 0.75**
LAM2	LAM2a	43.772841	3.317814	425	0.37	550.02 ± 99.87	21.82 ± 0.55	1.56 ± 11.8	1.24 ± 0.25	2.37 ± 1.44
(Scarp) LHD	LAM2b	43.772736	3.317936	425	0.37	624.9 ± 100.94	22.04 ± 0.56	2.26 ± 11.5	2.05 ± 0.38	5.72 ± 2.22
	LAM2c	43.772813	3.317942	425	0.35	557.17 ± 85.21	21.86 ± 0.63	3.68 ± 8	3 ± 0.47	12.6 ± 3.68
									Mean	**6.9 ± 2.44**
MM1	MM1a	43.759838	3.295386	530	0.45	294.11 ± 37.54	21.78 ± 0.56	2.72 ± 9.4	1.21 ± 0.17	4.33 ± 1.18
(Slide mass) LHD	MM1b	43.759822	3.295361	530	0.45	303 ± 52.46	21.58 ± 0.55	2.64 ± 9.1	1.18 ± 0.21	4.35 ± 1.44
	MM1c	43.759744	3.295239	530	0.45	321.08 ± 30.89	21.89 ± 0.57	2.02 ± 10.7	1.06 ± 0.14	3.41 ± 0.99
									Mean	**4.04 ± 1.2**
MM2	MM2a	43.759730	3.295186	535	0.58	432.05 ± 74.56	21.59 ± 0.56	2.26 ± 9.2	1.42 ± 0.25	3.08 ± 1.1
(Slide mass)	MM2b	43.759875	3.295419	535	0.5	434.51 ± 86.64	21.69 ± 0.55	2.6 ± 9.3	1.63 ± 0.33	4.43 ± 1.62
LHD	MM2c	43.759875	3.295419	535	0.5	382.14 ± 66.61	21.52 ± 0.55	2.62 ± 9	1.44 ± 0.26	4.26 ± 1.42
									Mean	**3.92 ± 1.38**

The type of surfaces sampled is indicated and acronyms are employed to indicate the lithology (*EHM* Early Hettangian Mudstone, with a density of 2.7 g.cm^{-3}, and *LHD* Late Hettangian Dolomite, with a density of 2.5 g.cm^{-3}). The depth of the samples is o m, and the thickness of the samples is 3 cm

Fracturing surveys were performed in the slide mass and outcrops in place (Fig. 2b). Outcrops in place exhibit two strike peaks. The first one corresponds to a strike of 070°–080°, and the second one is about 170°–180°. In the slide mass, one peak stands out about 070°–080°, with few measurements in Late Hettangian rocks showing a strike between 140° and 150° (Fig. 2b). The last ones are consistent with the depression orientation. Other fractures compatible with the depression with 110°N and 130°N have also been recognized on the hillshade upwards along the rock cliff.

The E-W set of fractures does not agree with the landslide-induced motion. Instead, it could have been responsible for the disintegration of the slide mass. In the western boundary, the strike of the bedding planes is 170° and appears to rotate clockwise compared to bedding planes in the slide mass. This rotation coincides with the orientation of the dry ravine and developed along a low throw fault as shown in Fig. 2a. The combination of the ravine and the fault plays as a lateral ramp of the Mont Mayres landslide and defines clearly its western boundary. The eastern boundary, is on the contrary, not visible. Based on these geomorphological features, a geological cross-section has been proposed (Fig. 2d).

Exposures ages

The natural chlorine values of the sampled rocks range from 129 to over 625 ppm (Table 1). We observed a correlation between the natural chlorine content and the nature of the rock: Lower Hettangian limestones contain less than 200 ppm chlorine (sample LAM1), whereas chlorine in dolomites varies between 294 and 625 ppm (Table 1). Natural chlorine is a source of ^{36}Cl production, and its high concentration affects the interpretation of the ages obtained. We can set a threshold of 500 ppm of natural chlorine, beyond which the exposure ages will be considered untrustworthy. One site exceeds this limit, as in LAM2. In contrast, the ages corresponding to low levels of natural chlorine (LAM1) are more reliable and have a lower error.

Looking at the probability density of exposure ages in Fig. 3, we see one cluster of ages. This group corresponds to the LAM1, MM1, and MM2 sites with mean ages of 4.01 ± 0.75, 4.04 ± 1.2, and 3.92 ± 1.38, respectively. The mean age for the entire group is 3.99 ± 1.11 ka.

Discussion and conclusions

LiDAR data and field investigations in the two investigated landslides in the Laurounet and Le Ricardenc valleys permitted us to recognize the upper part of two landslide structures. The Lamerallède and Mont Mayres landslides share the following characteristics. Their upper part comprises a slide mass including the stiff Hettangian units dipping downslope (25–40°), indicating a downward rotation of the mobilized rock slide. Slightly dipping rock slices separate the intact cliff from the slide mass within a depression zone, particularly in Mont Mayres. The vertical offset of the two landslides is similar and equals 15–20 m. We interpret that Lamerallède and Mont Mayres landslides correspond to rock spreading processes (Varnes 1978; Dikau et al. 1996; Pasuto and Soldati 2013; Hungr et al. 2014).

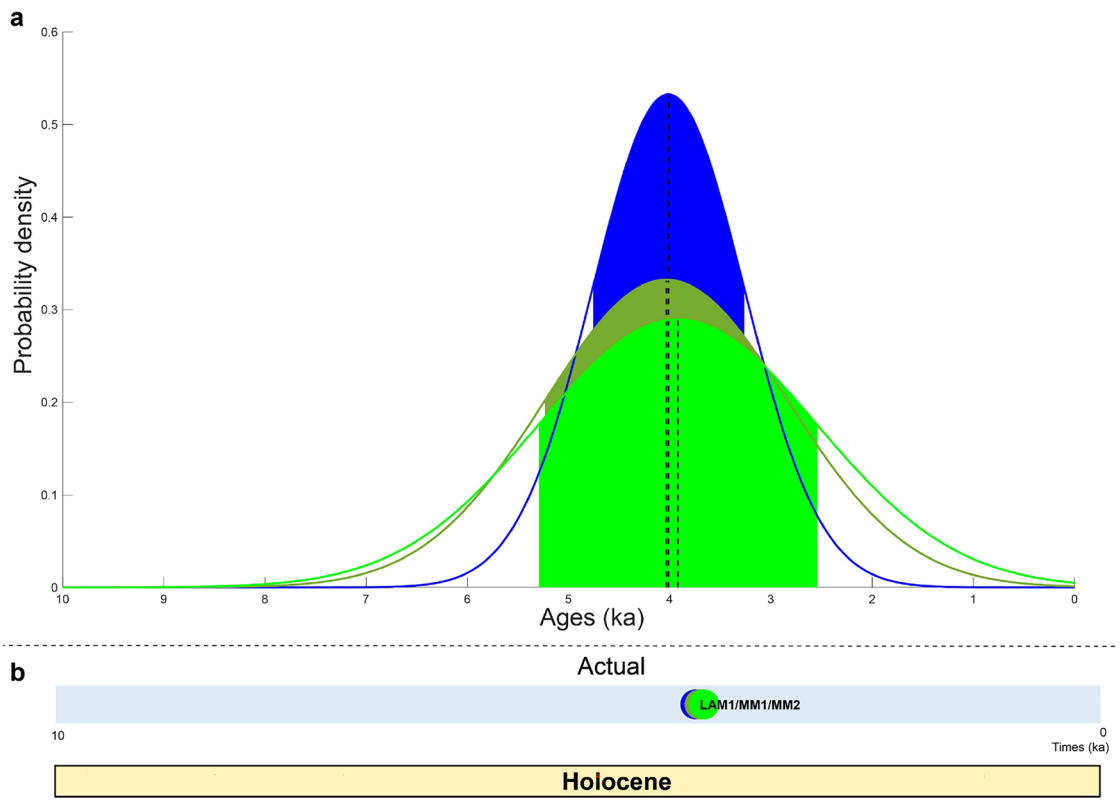

Fig. 3 **a** The mean age distribution for each sampling site except LAM2. **b** Timeline with averages for each sampling site except LAM2

Rock spreading is defined by a lateral extension of stiff (brittle) geological units (e.g. carbonates) overlying a soft (ductile) terrain (e.g. clays) that creeps. Such gravitational processes have been recognized in the peri-Mediterranean mountains, such as the Marbrière landslide in the French Maritime Alps (Zerathe and Lebourg 2012) the Peracalç landslide in Spanish Pyrenees (Gutierrez et al. 2012), the Il-Prajjet landslide in Malta (Mantovani et al. 1996), and the Mt. Reschberg landslide in Austria (Tung et al. 2021). These landslides are interpreted by a lateral expansion of the unconfined clay responsible for the subsidence of the carbonate part, accompanied in some cases by bulging (Zerathe and Lebourg 2012; Gutierrez et al. 2012; Pasuto and Soldati 2013). A bulge, i.e. a typical positive topographic expression, is related to clay creeping (Radbruch-Hall 1978; Pasuto and Soldati 2013). On the Lamerallède landslide toe, the bulge height is of the same order of magnitude as the landslide offset (~ 15 m). We propose that the forward rotation of the mobilized Hettangian-Rhaetian rocks in the Lamerallède and Mont Mayres landslides is associated with toppling (Varnes 1978; Dikau et al. 1996; Hungr et al. 2014) favoured by the inherited dense fracture network (Fig. 2).

The structural inheritance plays an important role in both landslides. Notably, the strike of the toppling movement is not aligned with the slope of the Lamerallède landslide, whereas it is in the Mont Mayres landslide. In the first one, the ~ N340° dip direction of the beds (with a 20°N–30°N inclination) is oblique to the 045° dip direction of the slope. Rock mass may thus be mobilized along a direction at an angle up to 30° relative to the slope direction. This obliquity can be explained by the regional 070° dense fracture set that pre-cut the stiff Hettangian units. This network seems to play a minor role in the Mont Mayres landslide, at least concerning the direction of the toppling movement. The western border of the Mont Mayres coincides with an N-S fault where reactivation is suggested with bed rotation close to the fault. These observations highlight the complexity of understanding the relative importance of inherited discontinuities and the 3D aspect of predisposing factors.

In addition to having a similar motion, these two landslides have similar ages, indicating a synchronous character. The average age of the landslides scarps is 3.99 ± 1.11 ka from samples at LAM1, MM1, and MM2 sites. Therefore, the Lamerallède and Mont Mayres landslides were triggered simultaneously. Although correlations with Holocene climatic conditions are somewhat speculative due to the large uncertainties of the dating method, we hypothesize that intense rainfalls would have occurred in the study area, inducing high lake levels in southern Europe at 4000 cal. a BP (Magny et al. 2011). This would point to precipitation and hydraulic charge as a potential triggering mechanism and the fracturing of the Larzac plateau, together with the lithologic contrast between the brittle carbonate overlying ductile clays and tectonic inherited discontinuities, as the potential predisposing factors for the investigated landslides. Presumably, these two landslides are two examples from the southern edge of the Larzac plateau that can be linked to climatic triggers.

Moreover, the fractures can also favour the subsidence movement with creep by water percolation, decreasing the weaker material's resistance. Indeed, water percolation may cause clay softening (Gutierrez et al. 2012; Pasuto and Soldati 2013), which in turn may increase the continuous deformation of the clays due to valley cutting, leading to the subsidence of the brittle formation. The development of shear zones in the clays is known to favour lateral expansion. Their identification is generally difficult due to the poor outcrop conditions. The water percolation can also dissolve evaporites and favour shearing surfaces, subsiding them by a collapse of the old location where evaporites dissolved (Gutierrez et al. 2012; Pasuto and Soldati 2013). Evaporitic dissolution by water percolation can also be related to karstification of the rock mass (Ambert and Ambert 1995; Gutierrez et al. 2012).

It would be interesting in the future to look at the possible evolution of this type of instability, particularly, by comparing it with other paleo-landslides in the region. It is generally accepted that lateral spreading can evolve into different modes of failure, such as rotational and translational landslides.

Acknowledgements

The authors thank the ASTER team especially Regis Braucher and Vincent Godard at CEREGE (Aix-en-Provence, France) for furnishing the essential chemistry measurements required for age calculations and discussion about exposure age results. Additionally, the authors would like to thank SARM (Nancy, France) for performing a comprehensive chemical analysis of the samples. The authors are grateful to the ANR-17-CE03-004-01 project, the "coup de pouce" project of ISTeP Sorbonne University, and the doctoral fellowship of the French Research Ministry for the financing of this study. To finish, we want to thank OSU "Ecce Terra" for using LiDAR drone material through the DROLI project. The DROLI lidar-drone is supplied by the Earth-Sea-Soils equipment pool of the OSU ECCE TERRA (UAR 3455). The authors also thank the two anonymous reviewers for their pertinent comments.

Data availability

Data is contained with the article or supplementary material.

Declarations

Conflict of interest The authors declare no competing interests.

References

Ambert M, Ambert P (1995) Karstification des plateaux et encaissement des vallées au cours du néogène et du Quaternaire dans les Grands Causses méridionaux (Larzac, Blandas). Géologie Fr 4:37–50

Azañón JM, Azor A, Pérez-Peña JV, Carrillo JM (2005) Late Quaternary large-scale rotational slides induced by river incision: the Arroyo de Gor area (Guadix basin, SE Spain). Geomorphology 69:152–168. https://doi.org/10.1016/j.geomorph.2004.12.007

Clague JJ (2015) Chapter 10 - Paleolandslides. In: Shroder JF, Davies T (eds) Landslide hazards, risks, and disasters. Academic Press, Boston, pp 321–344

Denchik N, Gautier S, Dupuy M et al (2019) In-situ geophysical and hydro-geochemical monitoring to infer landslide dynamics (Pégairolles-de-l'Escalette landslide, France). Eng Geol 254:102–112. https://doi.org/10.1016/j.enggeo.2019.04.009

Dikau R, Brundsen D, Schrott L, Ibsen M-L (1996) Landslide recognition: identification, movement and causes. John Wiley & Sons

Dunai TJ (2010) Cosmogenic nuclides: principles, concepts and applications in the earth surface sciences. Cambridge University Press, Cambridge

Dunai TJ, Stuart FM (2009) Reporting of cosmogenic nuclide data for exposure age and erosion rate determinations. Quat Geochronol 4:437–440. https://doi.org/10.1016/j.quageo.2009.04.003
Dunne J, Elmore D, Muzikar P (1999) Scaling factors for the rates of production of cosmogenic nuclides for geometric shielding and attenuation at depth on sloped surfaces. Geomorphology 27:3–11. https://doi.org/10.1016/S0169-555X(98)00086-5
Francioni M, Stead D, Clague JJ, Westin A (2017) Identification and analysis of large paleo-landslides at Mount Burnaby. Environ Eng Geosci, British Columbia. https://doi.org/10.2113/EEG-1955
Gutierrez F, Linares R, Roque C et al (2012) Investigating gravitational grabens related to lateral spreading and evaporite dissolution subsidence by means of detailed mapping, trenching, and electrical resistivity tomography (Spanish Pyrenees). Lithosphere 4:331–353. https://doi.org/10.1130/L202.1
Hungr O, Leroueil S, Picarelli L (2014) The Varnes classification of landslide types, an update. Landslides 11:167–194. https://doi.org/10.1007/s10346-013-0436-y
Magny M, Bossuet G, Ruffaldi P et al (2011) Orbital imprint on Holocene palaeohydrological variations in west-central Europe as reflected by lake-level changes at Cerin (Jura Mountains, eastern France). J Quat Sci 26:171–177. https://doi.org/10.1002/jqs.1436
Mantovani F, Soeters R, Van Westen CJ (1996) Remote sensing techniques for landslide studies and hazard zonation in Europe. Geomorphology 15:213–225. https://doi.org/10.1016/0169-555X(95)00071-C
Margielewski W (2006) Structural control and types of movements of rock mass in anisotropic rocks: Case studies in the Polish Flysch Carpathians. Geomorphology 77:47–68. https://doi.org/10.1016/j.geomorph.2006.01.003
Mather AE, Griffiths JS, Stokes M (2003) Anatomy of a 'fossil' landslide from the Pleistocene of SE Spain. Geomorphology 50:135–149. https://doi.org/10.1016/S0169-555X(02)00211-8
Pasuto A, Soldati M (2013) 7.25 Lateral spreading. Treatise on Geomorphology. Elsevier, pp 239–248
Radbruch-Hall DH (1978) Gravitational creep of rock masses on slopes. Developments in Geotechnical Engineering. Elsevier, pp 607–657
Schimmelpfennig I, Benedetti L, Finkel R et al (2009) Sources of in-situ 36Cl in basaltic rocks. Implications for calibration of production rates. Quat Geochronol 4:441–461. https://doi.org/10.1016/j.quageo.2009.06.003
Shultz CH, Harper JA (2002) "Fossil" and recent landsliding in Allegheny County. Pa Geol 32:8–15
Stead D, Eberhardt E, Coggan JS (2006) Developments in the characterization of complex rock slope deformation and failure using numerical modelling techniques. Eng Geol 83:217–235. https://doi.org/10.1016/j.enggeo.2005.06.033
Stone JO (2000) Air pressure and cosmogenic isotope production. J Geophys Res Solid Earth 105:23753–23759. https://doi.org/10.1029/2000JB900181
Stone JO, Allan GL, Fifield LK, Cresswell RG (1996) Cosmogenic chlorine-36 from calcium spallation. Geochim Cosmochim Acta 60:679–692. https://doi.org/10.1016/0016-7037(95)00429-7
Taboada A, Ginouvez H, Renouf M, Azemard P (2017) Landsliding generated by thermomechanical interactions between rock columns and wedging blocks: study case from the Larzac Plateau (Southern France). EPJ Web Conf 140:14012. https://doi.org/10.1051/epjconf/201714014012
Tung BD, Do NH, Thanh NK et al (2021) Geometry and the mechanism of landslide occurrence in a limestone area – case examples of landslides in Vietnam and from Europe, China, and Japan. J Disaster Res 16:646–657. https://doi.org/10.20965/jdr.2021.p0646
Varnes DJ (1978) Slope movement types and processes. In: Schuster RL, Krizek RJ (eds) Landslides, analysis and control, transportation research board, Special Report No. 176. National Academy of Sciences, pp 11–33
Zaruba Q, Mencl V (1982) Landslides and their control, 2nd completely rev. ed. Elsevier Scientific Pub. Co, Amsterdam ; New York : [Distributor] for the U.S. and Canada, Elsevier/North Holland
Zerathe S, Lebourg T (2012) Evolution stages of large deep-seated landslides at the front of a subalpine meridional chain (Maritime-Alps, France). Geomorphology 138:390–403. https://doi.org/10.1016/j.geomorph.2011.10.006

Supplementary Information The online version contains supplementary material available at https://doi.org/10.1007/s10346-024-02329-2.

Kévin Elkharrat (✉) · **Catherine Homberg** · **Sara Lafuerza** · **Nicolas Loget**
Institut des Sciences de la Terre de Paris (ISTeP), Sorbonne Universite, CNRS-INSU, 75005 Paris, France
Email: kevin.elkharrat@sorbonne-universite.fr

Muriel Gasc-Barbier
GeoCod, Cerema Méditerranée, 13593 Aix-en-Provence, France

Stephanie Gautier
University of Montpellier, Géosciences Montpellier — CNRS, Montpellier, France